

Feasibility study of nanocrystalline cellulose as adsorbent of steryl glucosides from palm-based biodiesel



Liangna Widdyaningsih^{a,1}, Albert Setiawan^{a,1}, Shella Permatasari Santoso^{a,b}, Felycia Edi Soetaredjo^{a,b}, Suryadi Ismadji^{a,b}, Sandy Budi Hartono^a, Yi-Hsu Ju^{b,c,d}, Phuong Lan Tran-Nguyen^e, Maria Yuliana^{a,*}

^a Department of Chemical Engineering, Widya Mandala Catholic University Surabaya, Kalijudan 37, Surabaya, 60114, Indonesia

^b Department of Chemical Engineering, National Taiwan University of Science and Technology, 43 Keelung Road, Sec 4, Taipei, 10607, Taiwan

^c Graduate Institute of Applied Science and Technology, National Taiwan University of Science and Technology, 43 Keelung Road, Sec 4, Taipei, 10607, Taiwan

^d Taiwan Building Technology Center, National Taiwan University of Science and Technology, 43 Keelung Road, Sec 4, Taipei, 10607, Taiwan

^e Department of Mechanical Engineering, Can Tho University, 3-2 Street, Can Tho City, Viet Nam

ARTICLE INFO

Article history:

Received 16 October 2019

Received in revised form

3 February 2020

Accepted 1 March 2020

Available online 4 March 2020

Keywords:

Biodiesel

Stery glucosides removal

Nanocrystalline cellulose

Adsorption isotherm

Adsorption mechanism

Feasibility study

ABSTRACT

Increasing the content of biodiesel in the diesel fuel mixture faces some challenges due to the presence of steryl glucosides (SG) compounds, which causes the filter clogging and the reduction of engine power. In this study, coarse filter paper-based nanocrystalline cellulose (CFP-based NCC) with the crystallinity of 85.73% is selected as a potential adsorbent to separate SG compounds in palm-based biodiesel (PO-B100). The adsorption experiments were carried out at various CFP-based NCC to PO-B100 mass ratio (1:50, 1:75, 1:100, 1:125, 1:150, 1:175, 1:200) and temperature (65, 75, 85 °C). The maximum SG removal was 91.81%, obtained at 75 °C for CFP-based NCC to PO-B100 mass ratio of 1:50. The adsorption treatment also improves the cold stability of PO-B100 by reducing the cloud point from 13.2 °C to 11.5 °C. Langmuir isotherm model is best-fitted to the equilibrium adsorption data and thermodynamic studies suggested that the adsorption of SG onto the CFP-based NCC surface is spontaneous and endothermic. The isotherm and thermodynamic study showed that the mechanism governing the adsorption process may be driven by both dipole-dipole interactions and ion exchange. The adsorption results showed that CFP-based NCC has great affinity and selectivity to SG and can be considered as a promising adsorbent of SG.

© 2020 Elsevier Ltd. All rights reserved.

1. Introduction

To date, petroleum diesel is used worldwide for transportation, manufacturing, power generation, construction and farming industries. However, disruption in crude market price and the long-term availability along with the nature deterioration due to its gas emission have become the major concerns for environmental sustainability [1]. Therefore, it is necessary to develop alternative fuels that are environmentally friendly, especially as a substitute for diesel fuel.

Of the several alternative fuels available, biodiesel is an alternative diesel fuel made from renewable biological resources [2].

Biodiesel is generally derived from transesterification of agricultural or animal lipids and short-chain alcohols in the presence of a catalyst. Conventional base-catalyzed transesterification in a batch stirred-tank reactor is the most common technique used to produce the commercially available biodiesel [3]. Several modifications on the conversion route as well as the reactor configuration and design have been performed in order to create, optimize and intensify the continuous production of biodiesel. The transesterification using catalyst-free subcritical [4–6] or supercritical alcohol [7,8], as well as heterogeneous [9] or enzymatic catalyst [9,10], gain wide attention in improving the continuity of biodiesel production. Likoza et al. (2016) also introduced a simple and robust design of a tubular reactor with a static mixer to intensify the mass transfer rate between the reactants and increase the biodiesel conversion rate. Their work also studied the chemical equilibrium and reaction kinetics at different operating parameters to optimize the product

* Corresponding author.

E-mail address: mariayuliana@ukwms.ac.id (M. Yuliana).

¹ These authors contributed equally to this work.

Abbreviation

SG	Steryl glucoside(s)
MG	Monoacylglyceride(s)
DG	Diacylglyceride(s)
TG	Triacylglyceride(s)
CFP	Coarse filter paper
NCC	Nanocrystalline cellulose
FAME	Fatty Acid Methyl Ester(s)
PO-B100	Palm-based biodiesel

yield [11].

While biodiesel is currently mass-produced and a large number of studies have been carried out to improve its performance in various aspects, the white precipitates are still a challenge for its manufacturers. Although biodiesel distributed around the country must conform to the fuel property specifications as controlled by ASTM D6751, white precipitates were often detected in biodiesel and its blends during storage [12]. Several cases even showed that suspended particles in biodiesel have been found shortly after the production and at a rather high temperature (slightly below 60 °C) [13]. The white precipitates may cause filter plugging in engine systems [13,14]. This phenomenon was also observed in many biodiesel plants and hence frequent maintenance and process modification are often essential to maintain plant effectiveness and efficiency.

The presence of sterol glucosides (SG), which is one of the plant sterols, has been identified as the major component of the white precipitates. It mostly presents in biodiesel with a concentration of 35 ppm or higher [15]. The existence of this dispersed particles of SG promotes the aggregation of other components in biodiesel, saturated monoacylglycerides (MG) and diacylglycerides (DG), and subsequently affects the cold flow stability of fuel and widespread use [16].

Several techniques have been conducted to minimize the SG content in the biodiesel product, namely enzymatic hydrolysis [17,18], adsorption using magnesium silicate and bleaching earth [16] and ultrafiltration [19]. SG removal by enzymatic hydrolysis resulted in 81% removal efficiency with the addition of a synthetic codon-optimized version of the LacS gene expressed from *E. coli* with the total operating time of 7 h [17]. Na-Ranong et al. (2015) reported that the conventional adsorption using magnesium silicate and bleaching earth in temperature of 65–80 °C yielded in 81.4–82.5% removal efficiency of SG [16]. Tremblay and Montpetit (2017) stated that the highest separation for SG (86%) by ultrafiltration was obtained when the biodiesel was transesterified using 0.7% (w/w) catalyst and 4:1 methanol:soybean oil molar ratio [19]. Based on the removal efficiency and economic feasibility, the adsorption treatment is a potential method to reduce SG content as well as to improve the cold flow properties of the fuel in the industrial scale because it is found to be effective and facile, time-saving and energy-efficient.

The development of adsorbent for effective adsorption has been conducted using various types of materials. Currently, the development of cellulosic adsorbent received major interest because it is renewable, biodegradable, low cost, and non-toxic [20]. Cellulosic adsorbents have the ability to meet the requirement of being a biosorbent, as it is abundantly available as a natural biopolymer. Cellulose in the form of nanocrystalline cellulose (NCC) has been widely studied due to its extensive industrial application, namely enzyme immobilization, adsorption, catalysis, drug delivery, biosensors and bio-imaging [21]. NCC, with a large specific surface area

and plenty of surface hydroxyl and anionic sulfate ester group for physical and chemical reactions [22–24], can be considered as a new promising adsorbent for SG removal.

As the Indonesian government plans to increase the use of biodiesel in diesel blend from B20 to B30 in the time span of 5 years, the use of NCC for SG removal and improvement of the cold stability is an interesting topic to be studied. The objective of this study is to observe the feasibility of coarse filter paper-based NCC (CFP-based NCC) as the adsorption agent for SG. Various operating parameters, namely temperature, and the mass ratio of CFP-based NCC to palm-based biodiesel (PO-B100) will be monitored. The adsorption mechanism was also proposed based on the isotherm and thermodynamics study.

2. Materials and methods

2.1. Materials

PO-B100 was collected from a local palm oil manufacturer in Gresik, Indonesia, and stored for 3 days at room temperature prior to the adsorption experiment. Coarse filter paper (CFP) as the cellulosic material was obtained from a local supplier in Surabaya, Indonesia. Sulphuric acid, sodium hydroxide, ethyl acetate, and n-hexane were purchased from Merck, Germany. FAMES standard 47885 U contains 37 components FAME mix and SG standard 1117 were procured from Supelco (Bellefonte, PA, USA) and Matreya (State College, PA, USA), respectively. Nitrogen gas (99.9% purity) was purchased from Aneka Gas Industry Pty. Ltd., Surabaya. All reagents were of analytical grade and required no further purification.

2.2. Preparation of NCC

CFP was ground into fibrous powder before use. The non-cellulosic material of CFP was subsequently removed to obtain purified cellulose using the modified method of Putro et al. (2017) [25]: 12 g of the CFP powder was delignified using 0.1 g/ml sodium hydroxide aqueous solution (40 ml). The delignified product was washed with distilled water and filtrated three times through a Whatman 1 (11 µm pore size) filter paper before being dried under vacuum at 80 °C for 12 h.

CFP-based NCC was prepared by using acid hydrolysis following the procedure conducted by Putro et al. (2017) [25]. 1 g of delignified cellulose was hydrolyzed with 20 ml sulphuric acid 64% at 45 °C for 75 min under constant agitation. The reaction time was selected to ensure high reaction efficiency. After the specified duration, the reaction was immediately quenched using 20-fold of cold distilled water. The suspension was centrifuged at 4500 rpm for 10 min to remove the excess acid solution. The resulting precipitates were dialyzed against distilled water until neutral pH was achieved. The colloidal suspension was subjected to sonication treatment for 30 min in a cooling bath to avoid overheating and subsequently subjected to vacuum drying at 80 °C for 6 h to obtain CFP-based NCC powder.

2.3. Characterization of CFP-based NCC

The surface morphologies of the CFP-based NCC particles were analyzed on a field emission scanning electron microscope (FESEM) JEOL JSM-6500F (Jeol Ltd., Japan), with an accelerating voltage of 5–10 kV and 9.5–9.6 mm working distance. The CFP-based NCC powder was attached to a stub, sputtered and coated with gold prior to analysis. Fourier Transform Infrared (FTIR) analysis was performed by an FTIR-8400S spectrophotometer (Shimadzu, Japan) in the range of 400–4000 cm⁻¹ at a 4 cm⁻¹ scanning resolution.

XRD analysis was conducted by an X'PERT Panalytical Pro X-Ray diffractometer (Philips-FEI, Netherlands) with monochromatic Cu $K\alpha_1$ radiation at wavelength (λ) = 0.154 nm, 40 kV of voltage and 30 mA of tube current. The diffraction pattern was acquired in the range of 5°–60° (2θ angle). The crystallinity index (CrI) was expressed according to the following equation, as proposed by Segal et al. (1959) [26].

$$\text{CrI (\%)} = \frac{(I_{200} - I_{\text{am}})}{I_{200}} \times 100 \quad (1)$$

Where I_{200} is the maximum intensity of the 200 lattice diffraction at 2θ around 22°, I_{am} is the maximum intensity of the amorphous region at $2\theta = 18^\circ$. The crystallite size (nm) was calculated using the Scherrer analysis.

2.4. Compositional study of SG in PO-B100 using GC-FID analysis

The analysis of SG composition in PO-B100 was carried out using GC-17A (Shimadzu, Japan), completely equipped with a split/splitless injector and a flame ionization detector (FID). The separation was performed using nonpolar capillary column DB-5HT (5 %-phenyl)-methylpolysiloxane (15 m \times 0.32 mm ID, Agilent Technology, CA). The column temperature was initially set at 80 °C, then subsequently ramped to 365 °C at the rate of 15 °C/min, and held constant for 19 min. The temperature of the injector and detector were adjusted constant at 370 °C 100 mg of SG was dissolved in 1 ml ethyl acetate and subjected to filtration using polyvinylidene difluoride (PVDF) filter prior analysis. The prepared sample (1 μ l) was injected into the GC with a split ratio of 1:50. The velocity of nitrogen (N_2 , 99.9%) as the carrier gas was fixed at 30 cm/s at 80 °C.

2.5. Removal of SG using adsorption

The adsorption of SG from PO-B100 was conducted in a batch mode according to the study conducted by Na-Ranong et al. (2015) with a few modifications [16]. A various mass ratio of CFP-based NCC to PO-B100 (1:50, 1:75, 1:100, 1:125, 1:150, 1:175, 1:200) was introduced into a series of beakers, where the mixture will be subjected to a 1-h adsorption process at constant temperature and agitation speed (250 rpm). The selection of adsorption duration was based on the preliminary experiment conducted to find the equilibrium time. Several adsorption temperatures (65, 75 and 85 °C) were used to study the effect of temperature on the adsorption of SG. The solution was separated from the adsorbent by using centrifugation at the rotational speed of 4900 rpm for 10 min. The SG contents in PO-B100 before and after adsorption were analyzed using UV-mini 1240 spectrophotometer (Shimadzu, Japan) at 240 nm, according to the modified technique conducted by Moreau et al. (2008), Nyström (2007) and Araújo et al. (2013) [14,27,28]. The percentage of SG removal was determined by using the following equation.

$$\text{SG removal (\%)} = \frac{C_i - C_f}{C_i} \times 100 \quad (2)$$

Where C_i is the concentration of SG in untreated PO-B100 (mg/kg) and C_f is the concentration of SG in treated (after adsorption) PO-B100 (mg/kg). The results of SG removal were verified by using GC-FID analysis (see section 2.4) and its statistical approach was performed using Minitab software (version 18.1) to identify the significance order of the parameters affecting the adsorption.

2.6. Isotherm and thermodynamics study of the SG adsorption

The adsorption isotherm was conducted at the temperature of 65, 75 and 85 °C with various CFP-based NCC to PO-B100 mass ratio (1:50, 1:75, 1:100, 1:125, 1:150, 1:175, 1:200). It was performed using a similar procedure as previously mentioned in subsection 2.5. At the equilibrium condition, the amount of adsorbed SG per unit mass of CFP-based NCC as the adsorbent (Q_e) was calculated by the equation below.

$$Q_e \left(\frac{\text{mg}}{\text{g}} \right) = \frac{C_0 - C_e}{m} \times V \quad (3)$$

Where C_0 and C_e are the initial and final (equilibrium) concentration of SG in PO-B100 (mg/L), respectively, m is the mass of adsorbent (g) and V is the volume of PO-B100 (L).

The equilibrium data obtained at various temperature were fitted to the three isotherm models, namely Langmuir, Freundlich and Dubinin-Radushkevich (D-R). Meanwhile, the thermodynamic parameters such as Gibbs free energy change (ΔG°), enthalpy (ΔH°) and entropy (ΔS°) were further determined from the results of isotherm study using equations (4) and (5).

$$\Delta G^\circ = -RT \ln \left(K_L \cdot M_{SG} \cdot 10^3 \cdot C^0 \right) \quad (4)$$

$$\Delta G^\circ = \Delta H^\circ - T \Delta S^\circ \quad (5)$$

Where R is the gas constant with the value of 8.314 J/mol.K, T is the absolute temperature in Kelvin, K_L is Langmuir equilibrium constant in L/mg, M_{SG} is the molecular weight of SG in g/mol and C^0 is the reference concentration in standard state with the value of 1 mol/L.

3. Results and discussions

3.1. Characterization of CFP-based NCC

The X-ray diffraction pattern of the CFP and its NCC are shown in Fig. 1, and the corresponding crystallinity index is presented in Table 1. Both XRD patterns showed the cellulose I characteristic peaks at 2θ around 15–17° (110 crystal plane) and 22–23° (200 crystal plane) [26,29]. The crystallinity index of CFP and its NCC were calculated using equation (1) and recorded to have the corresponding value of 57.60% and 85.73%. The change of crystallinity has occurred because of the progressive removal of amorphous hemicellulose and lignin during acid hydrolysis. The highly crystalline product is more efficient to improve the mechanical properties of the composite material, particularly as an adsorbent, since crystallinity positively corresponds to the tensile strength of the material [30].

The scanning electron micrograph in Fig. 2 shows the shape and size of the CFP-based NCC. The distribution of NCC products derived from CFP was estimated to have approximately 200–400 nm in length (Fig. 2). The prepared CFP-based NCC has a homogenous needle-shaped with crystallite size in the range of 2–4 nm, obtained from the combination of X-ray diffraction data and Scherrer analysis. The homogenous CFP-based NCC particles are likely caused by the swollen of cellulose fibers due to NaOH delignification pretreatment [25].

Fig. 3 (a) – (b) illustrated the FTIR spectra of CFP-based NCC before and after adsorption. As shown in Fig. 3 (a), several peaks representing certain functional groups in CFP-based NCC were found in the spectra. The broad band in the range of 3008–3459 cm^{-1} represents the O–H stretching vibrations, while

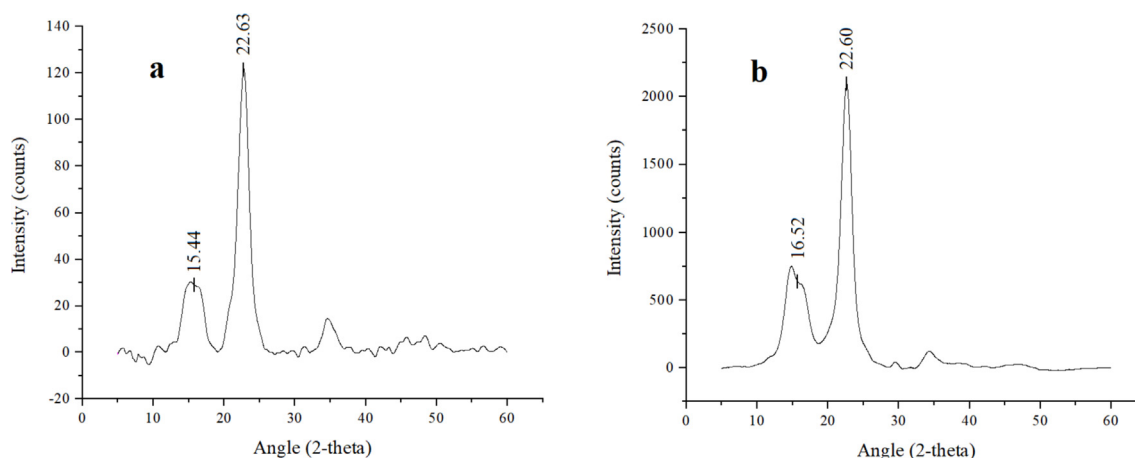


Fig. 1. X-ray diffraction patterns of (a) CFP, (b) CFP-based NCC.

Table 1
The crystallinity index of CFP and CFP-based NCC.

Samples	2-theta (°)		Crystallinity (%)
	110 crystal plane	200 crystal plane	
CFP	15.44	22.63	57.60
CFP-based NCC	16.52	22.60	85.73

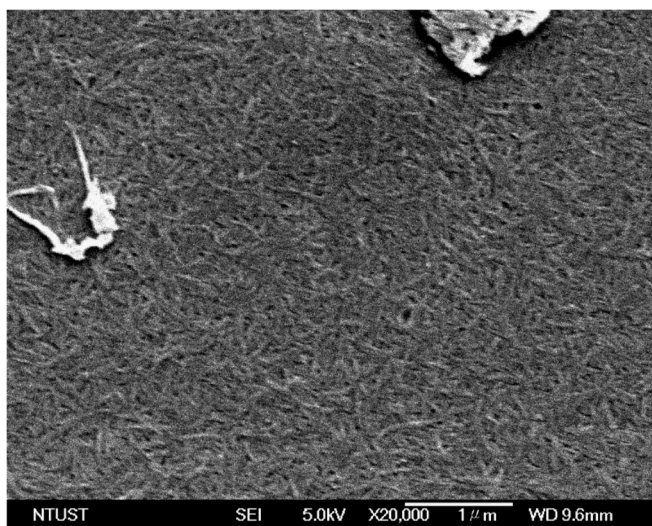


Fig. 2. SEM image of the rod-like CFP-based NCC particles.

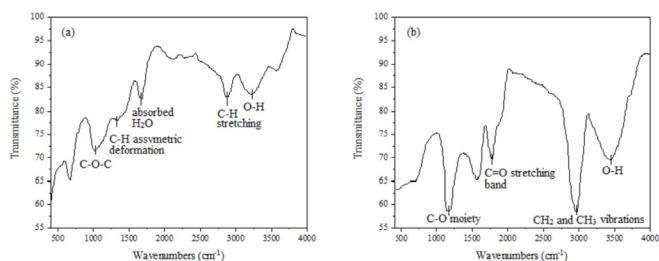


Fig. 3. FTIR spectrum of (a) CFP-based NCC before adsorption and (b) CFP-based NCC after adsorption.

the peaks in the range of 2802–2925 cm^{-1} correspond to C–H stretching vibrations. The absorption at 936–1137 cm^{-1} is related to the functional group of C–O–C, and the peak at 1640 cm^{-1} indicates the presence of abundant hydrophilic hydroxide group in the cellulose [31]. A peak at 1382 cm^{-1} represents the C–H asymmetric deformations [32].

Meanwhile, Fig. 3 (b) showed strong peaks in the wavenumbers of around 1019–1376 cm^{-1} and 2602–3160 cm^{-1} , which represent the C–O moiety, and CH_2 and CH_3 stretching vibrations. These two specific peaks are known as the fingerprint areas for SG. Another peak at 1750 cm^{-1} corresponds to the typical C=O stretching band of the methyl ester, while an O–H band around 3110–3700 cm^{-1} indicates the presence of hydroxyl groups in SG and CFP-based NCC [33]. Therefore, based on the FTIR spectra, it can be concluded that SG is the major component of the adsorbate on the surface of CFP-based NCC, which is consistent with the GC–FID results discussed in section 3.2.

3.2. Properties of PO-B100

The properties of PO-B100 have been analyzed according to the standard method of ASTM for its content of FAME, acid value (AV), MG, DG and triglycerides (TG). As reported in Table 2, the purity of FAME in PO-B100 is 98.7%, while the AV, MG, DG, and TG values are 0.12 mg KOH/g, 0.23%, 0.09%, and 0.06%, respectively. Furthermore, PO-B100 feedstock contained 194.1 mg/kg of SG with the cloud point of 13.2 °C and a clear initial appearance. Based on the GC–FID analysis, the SG profile in PO-B100 consists of 34.79% of campesteryl glucoside, 23.73% of stigmasteryl glucoside and 41.48% of β -sitosteryl glucoside. The results met the requirements of ASTM D6751 and SNI 7182:2015. However, white precipitates could be found within a few hours after production.

After the adsorption using the parameters giving the highest SG removal (1:50, 75 °C, 1 h; see section 3.3), the sample of treated PO-B100 was collected for the properties measurement in order to monitor the effect of the adsorbent. According to the results, the treated PO-B100 contained FAME with a purity of 98.8% and AV value of 0.11 mg KOH/g. The concentration of SG reduced significantly to 15.9 mg/kg with the composition of 24.81% campesteryl glucoside, 25.07% stigmasteryl glucoside and 50.12% β -sitosteryl glucoside, while the other glycerides components, MG, DG, and TG, were slightly decreased to 0.22%, 0.09%, 0.05%, respectively. The cloud point of the treated PO-B100 was also found to be decreased to 11.5 °C. These results indicated that CFP-based NCC has selectivity to adsorb SG, particularly campesteryl glucoside and

Table 2

The properties of untreated and treated PO-B100 (1:50, 75 °C, 1 h), and the comparison with ASTM D6751 and SNI 7182:2015.

Parameters	ASTM D6751	SNI 7182:2015	Untreated PO-B100	Treated PO-B100 (1:50, 75 °C, 1 h)
FAME (%)	≥96.5	≥96.5	98.7	98.8
AV (mg KOH/g)	≤0.50	≤0.50	0.12	0.11
MG (%)	≤0.80	≤0.80	0.23	0.22
DG (%)	≤0.20	–	0.09	0.09
TG (%)	≤0.20	–	0.06	0.05
SG (mg/kg)	N/A ^a	N/A ^a	194.1	15.9
Cloud point (°C)	–	18.0	13.2	11.5

^a Not available.

stigmasteryl glucoside, as compared to the other minor components, such as MG, DG, and TG. It also subsequently lowered the cloud point significantly, which is advantageous for storage and transportation purposes [34].

3.3. Adsorption of SG using CFP-based NCC

Fig. 4 summarized the SG removal rate at the various temperature and mass ratios of CFP-based NCC to PO-B100. The highest value of the SG removal rate (91.81%) was obtained at the following conditions: 75 °C, CFP-based NCC to PO-B100 mass ratio of 1:50, and 1 h adsorption time. Based on the results shown in Fig. 4, the lowest removal rate of SG in every adsorption temperature was seen at 1:200 of CFP-based NCC to PO-B100 mass ratio. It was likely due to insufficient binding and active adsorption sites and the adsorption required more time to reach the equilibrium stage. The removal percentage of SG was observed to have amplified with the increase of CFP-based NCC to PO-B100 mass ratio from 1:200 to 1:50 at all temperatures in the tested range. Greater amounts of CFP-based NCC provide greater adsorption surface area and active sites in CFP-based NCC, leading to an adequate SG binding area and certainly, a higher percentage of SG removal [35]. It was also monitored that the SG removal rate exponentially increased when the CFP-based NCC to PO-B100 mass ratio was increased from 1:100 to 1:50 in the all adsorption temperature. The phenomenon indicated the good dispersion ability of CFP-based NCC in PO-B100, where constant diffusion path length of SG binding to CFP-based NCC surface was found regardless of the amount of adsorbent [36].

As depicted in Fig. 4, temperature also remarkably affected the SG reduction. A temperature elevation from 65 °C to 75 °C improves

the reduction of SG, regardless of CFP-based NCC to PO-B100 mass ratio. Chowdhury et al. (2011) stated that the adsorption enhancement along with the temperature increase may be associated with the increase of the number of active sites available for adsorption. The diffusion rate of the adsorbate across the external boundary layer also escalates with the rise in temperature, due to lower solution viscosity and enhancement in the mobility and kinetic energy of the adsorbate [37]. Therefore, the collision between particles intensifies with the temperature elevation so that the activation energy of the adsorption process is easier to achieve. As a result, the amount of the adsorbed SG enhances along with the temperature increase. However, it was also observed that the SG removal rate decreased when the temperature was further escalated from 75 °C to 85 °C. More (2018) mentioned that after reaching a certain temperature, excessive particle collision causes the removal of adsorbates from the adsorbent, leading to lower adsorption capacity [38]. Lee et al. (2019) also stated that the NCC surface binding generally weakens along with the temperature enhancement [36]. The fluctuations of the SG uptake observed with the change in temperature suggests that the SG adsorption is governed by both physical attraction and chemical bonding, indicating that the sorption of SG by CFP-based NCC is both driven by physical and chemical sorption [37,39].

Fig. 5 presented the Pareto chart of the standardized effect generated using statistical analysis (Minitab version 18.1). The figure showed that both independent parameters (temperature and the mass ratio of CFP-based NCC to PO-B100) were found to be prominent with the significance order of the mass ratio of CFP-based NCC to PO-B100 > temperature. The other quadratic and two-way interaction terms were also found to significantly affect the SG removal rate.

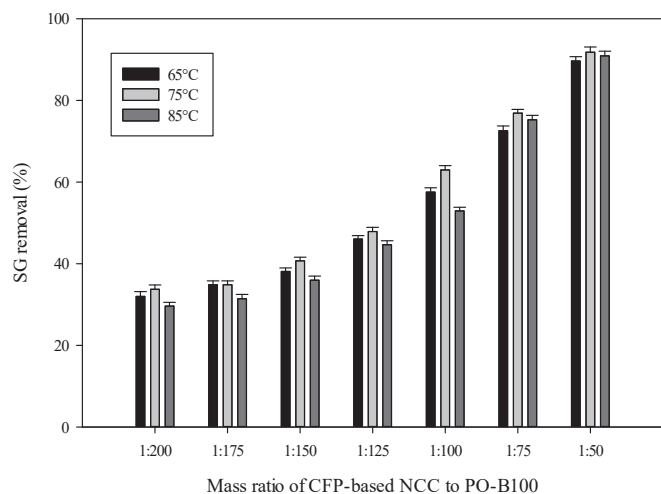


Fig. 4. SG removal rate varied with the mass ratio of CFP-based NCC to PO-B100 at three different temperatures.

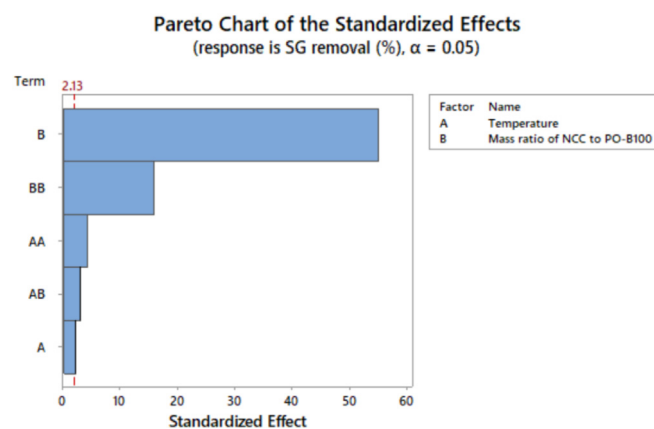


Fig. 5. The Pareto chart of the standardized effect showing the significance order of the two independent variables (temperature and mass ratio of NCC to PO-B100) on the SG removal, generated by ANOVA.

3.4. Study of adsorption isotherm and thermodynamic parameters

In this study, three isotherm equations were fitted to the experimental equilibrium data for SG at three temperature points (65 °C, 75 °C and 85 °C). The results are presented in Table 3 and the isotherm models are plotted in Fig. 6. The Langmuir isotherm constant, K_L and maximum absorption capacity, $Q_{m(L)}$ were calculated from the nonlinear curve fitting between Q_e and C_e . The value of $Q_{m(L)}$ was found to be increased from 12.50 mg/g at 65 °C to 12.93 mg/g at 75 °C before declining to 11.24 mg/g at the highest tested temperature (85 °C). The $Q_{m(L)}$ results are quite comparable to the adsorption capacity of magnesium silicate and bleaching earth on the SG (~13 mg/g) [16]. The Langmuir constant (K_L) also increases along with the temperature, from 0.11 L/mg at the lowest temperature (65 °C) to 0.26 L/mg at the highest temperature point (85 °C), indicating that the adsorption of SG to CFP-based NCC is an endothermic process.

The isotherm data were further analyzed by the Freundlich model. The Freundlich constant K_F and $1/n$ were obtained from the non-linear regression analysis. Table 3 showed that the values of $1/n$ are all under unity, ranging from 0.03 at 75 °C to 0.16 at 65 °C. The extent of $1/n$ represents the favorability degree of adsorption. The value of $1/n$ less than unity corresponds to favorable sorption. It was also observed that the Freundlich constant greatly escalates along with the temperature, implying that the adsorption was favorable at high temperature and the process is certainly endothermic. de Sá et al. (2017) mentioned that $1/n$ value between 0 and 1 is associated with a chemisorption process [40].

Another isotherm equation, the Dubinin-Radushkevich (D-R) model, was further applied to analyze the equilibrium data, particularly to determine the nature of SG adsorption onto CFP-based NCC surface. The D-R constant (β) gives an idea about the mean sorption energy, E , and their correlation can be expressed by the following equation:

$$E = \frac{1}{\sqrt{2\beta}} \quad (6)$$

where E represents sorption energy (kJ/mol) and β is the D-R constant (mmol^2/J^2). The value of sorption energy provides information to determine the type of adsorption mechanism, as chemical ion exchange or physical adsorption. Li et al. (2009) and Zhu et al. (2009) stated that if the sorption energy ranges from 8 to 16 kJ/mol, the sorption process is supposed to be chemisorption, while for energy value lower than 8 kJ/mol, the sorption is of physical nature [41,42]. Based on the results provided in Table 3, the adsorption mechanism is physical attraction since the E values for all tested temperatures are lower than 8 kJ/mol. The highest $Q_{m(D-R)}$ was found at 75 °C with a value of 12.13 mg/g, which was similar to

Table 3
Isotherm parameters of SG adsorption onto CFP-based NCC surface.

Isotherm	Parameters	Temperature (K)		
		338	348	358
Langmuir	$Q_{m(L)}$ (mg/g)	12.50	12.93	11.24
	K_L (L/mg)	0.11	0.16	0.26
	r^2	0.8587	0.8580	0.7039
	χ^2	0.2329	0.2865	0.2487
Freundlich	K_F ((mg/g) (L/mg) ^{1/n})	5.59	6.48	7.31
	$1/n$	0.16	0.03	0.09
	r^2	0.8408	0.7986	0.6079
	χ^2	0.2624	0.4064	0.3293
Dubinin-Radushkevich	$Q_{m(D-R)}$ (mg/g)	11.58	12.13	10.86
	E (kJ/mol)	0.18	0.25	0.29
	r^2	0.8094	0.8387	0.7555
	χ^2	0.3147	0.3254	0.2053

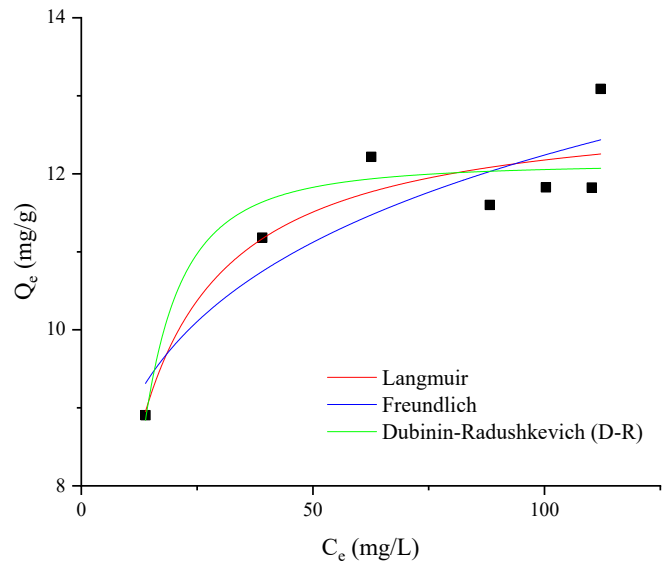


Fig. 6. The modelled isotherm profiles for the adsorption of SG to CFP-based NCC surface (temperature = 75 °C, mass ratio of CFP-based NCC to PO-B100 = 1:50, time = 1 h, agitation speed = 250 rpm).

the result obtained using Langmuir isotherm. The effect of temperature previously studied also provides similar results where the temperature of 75 °C gives the highest SG removal rate compared to the other tested temperatures.

The correlation coefficient (r^2) and chi-square (χ^2) values of the three isotherms are also listed in Table 3. It could be concluded that the adsorption of SG onto the CFP-based NCC surface is best fitted to the Langmuir isotherm equation under the temperature range studied. Based on the three isotherm models studied, the adsorption mechanism is predicted to be driven by both physical and chemical sorption due to its sorption energy value and endothermic nature, respectively. The overall results of this study showed that NCC has a particular affinity for SG and is an effective adsorbent for SG removal from PO-B100.

Table 4 listed the thermodynamics parameters of the SG adsorption onto the surface of NCC, such as Gibbs free energy change (ΔG°), enthalpy (ΔH°) and entropy (ΔS°). The values of Gibbs free energy (ΔG°) for the adsorption of SG were negative at all tested temperatures. These values confirm the spontaneous nature of SG adsorption onto the CFP-based NCC. Enhancement of the ΔG° value along with the increasing temperature implies that the affinity of SG on CFP-based NCC was higher at high temperature. Positive ΔH° value (42.90 kJ/mol) verifies that the adsorption is indeed an endothermic process, while the absolute value of ΔS° (219.80 J/mol.K) reflects the increased randomness at the solid-solution interface during the adsorption process [37,43].

3.5. Adsorption mechanism study

The study of the adsorption mechanism was used to further illustrate the interaction between SG and CFP-based NCC surface. Two important points have to be considered to understand the

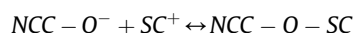
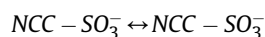
Table 4
Thermodynamic parameters of adsorption of SG onto CFP-based NCC surface.

Temperature (K)	Thermodynamic parameters		
	ΔG° (kJ/mol)	ΔH° (kJ/mol)	ΔS° (J/mol.K)
338	-31.44	42.90	219.80
348	-33.46		
358	-35.84		

mechanism, namely the surface properties of the adsorbent and the structure of adsorbate. The NCC molecule was constructed by a substantial number of hydrogen bonds between glucose units or glucose chains inside the molecule to form a very stable structure [44,45]. NCC contains the majority of oxygen functional groups such as hydroxyl, ether, and sulfonate. While the hydroxyl and ether groups are originally present in the cellulosic material, the sulfonate group existed due to the acid hydrolysis to produce NCC. On the other hand, SG was built by a steryl cation (SC^+) and a glucose unit, with a positive charge on the cationic steryl part.

According to the findings of this study, the adsorption was temperature-dependent and the isotherm modeling showed an equal contribution of physical attraction and chemical binding. Therefore, the mechanism of SG removal by adsorption on the CFP-based NCC surface may be presumed to involve these following steps:

- Migration of SG from the bulk of PO-B100 to the CFP-based NCC surface
- Diffusion of SG through the boundary layer to the CFP-based NCC surface
- Adsorption of SG on the surface of CFP-based NCC, which may be caused by physical interaction of dipole-dipole coupling between the positively charged SC^+ and the negatively charged NCC surface as suggested in Fig. 7; and through a possible chemical binding mechanism of ion exchange as shown below:



- Intraparticle diffusion of SG into the pores of CFP-based NCC

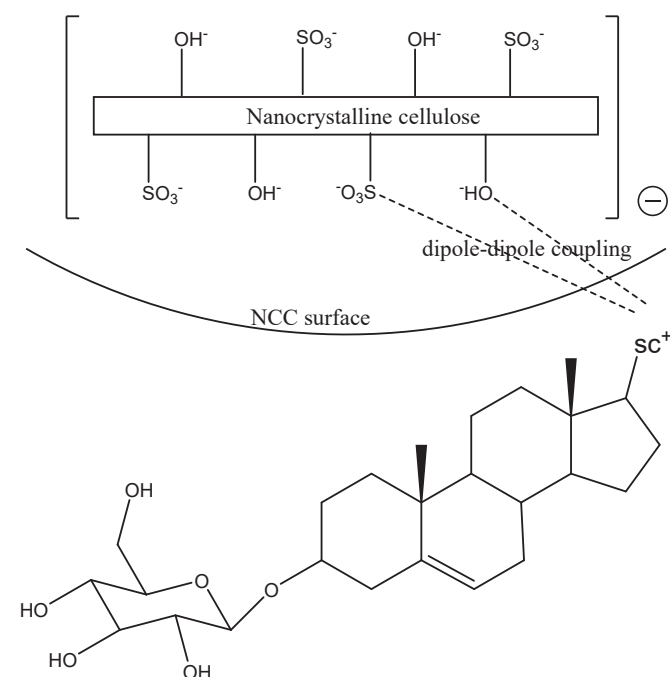


Fig. 7. Schematic representation of the proposed adsorption mechanism of SG onto CFP-based NCC surface.

4. Conclusions

CFP-based NCC was successfully used as an adsorbent for reducing SG in PO-B100. The content of SG was able to be reduced from 194.1 mg/kg to as low as 15.9 mg/kg (91.81% removal rate) within 1 h at the temperature of 75 °C using CFP-based NCC to PO-B100 mass ratio of 1:50. The study proved that CFP-based NCC has great affinity and selectivity to SG, particularly on the campesterol glucoside and stigmasteryl glucoside. The adsorption treatment greatly improves the cold stability of PO-B100 by reducing the cloud point from 13.2 °C to 11.5 °C, while slightly affected the purity of FAME, AV and other minor components, such as MG, DG, and TG, which were still in the acceptable range according to ASTM D6751. The adsorption process was endothermic and may be driven by both physical attraction and chemical ion exchange. The adsorption treatment using CFP-based NCC should be a prospective method used to remove SG from PO-B100 since it possesses high efficiency, time-saving and energy-efficient.

Declaration of competing interest

The authors declare that they have no known competing financial interests or personal relationships that could have appeared to influence the work reported in this paper.

CRediT authorship contribution statement

Liangna Widyanyingsih: Conceptualization, Methodology, Investigation, Software, Writing - original draft. **Albert Setiawan:** Conceptualization, Methodology, Investigation, Software, Writing - original draft. **Shella Permatasari Santoso:** Conceptualization, Data curation, Supervision. **Felycia Edi Soetaredjo:** Resources, Visualization. **Suryadi Ismadji:** Resources, Validation. **Sandy Budi Hartono:** Software, Validation. **Yi-Hsu Ju:** Writing - review & editing. **Phuong Lan Tran-Nguyen:** Writing - review & editing. **Maria Yuliana:** Conceptualization, Resources, Visualization, Writing - review & editing, Supervision.

Acknowledgment

This work was supported by Widya Mandala Catholic University Surabaya, Indonesia, through research grant no. 0675/WM01/N/2019.

References

- [1] N. Kumar, A. Sonthalia, H.S. Pali, Sidharth, Alternative Fuels for Diesel Engines: New Frontiers, Diesel Engines [Working Title], 2018, pp. 1–27, <https://doi.org/10.5772/intechopen.80614>.
- [2] A.C. Pinto, L.L.N. Guarieiro, M.J.C. Rezende, N.M. Ribeiro, A. Ednildo, Biodiesel: An Overview, 16, 2005, pp. 1313–1330.
- [3] Z. Qiu, L. Zhao, L. Weatherley, Process intensification technologies in continuous biodiesel production, Chem. Eng. Process. Process Intensif. 49 (2010) 323–330, <https://doi.org/10.1016/j.cep.2010.03.005>.
- [4] Y.H. Ju, L.H. Huynh, Y.A. Tsigie, Q.P. Ho, Synthesis of biodiesel in subcritical water and methanol, Fuel 105 (2013) 266–271, <https://doi.org/10.1016/j.fuel.2012.05.061>.
- [5] S. Thiruvankadam, S. Izhar, Y. Hiroyuki, R. Harun, One-step microalgal biodiesel production from Chlorella pyrenoidosa using subcritical methanol extraction (SCM) technology, Biomass Bioenergy 120 (2019) 265–272, <https://doi.org/10.1016/j.biombioe.2018.11.037>.
- [6] F.H. Santosa, L. Laysandra, F.E. Soetaredjo, S.P. Santoso, S. Ismadji, M. Yuliana, A facile noncatalytic methyl ester production from waste chicken tallow using single step subcritical methanol: optimization study, Int. J. Energy Res. 43 (2019) 8852–8863, <https://doi.org/10.1002/er.4844>.
- [7] M. Aghilinategh, M. Barati, M. Hamadani, Supercritical methanol for one put biodiesel production from chlorella vulgaris microalgae in the presence of CaO/TiO₂ nano-photocatalyst and subcritical water, Biomass Bioenergy 123 (2019) 34–40, <https://doi.org/10.1016/j.biombioe.2019.02.011>.
- [8] L.K. Ong, C. Effendi, A. Kurniawan, C.X. Lin, X.S. Zhao, S. Ismadji, Optimization

- of catalyst-free production of biodiesel from Ceiba pentandra (kapok) oil with high free fatty acid contents, *Energy* 57 (2013) 615–623, <https://doi.org/10.1016/j.energy.2013.05.069>.
- [9] M.K. Lam, K.T. Lee, A.R. Mohamed, Homogeneous, heterogeneous and enzymatic catalysis for transesterification of high free fatty acid oil (waste cooking oil) to biodiesel: a review, *Biotechnol. Adv.* 28 (2010) 500–518, <https://doi.org/10.1016/j.biotechadv.2010.03.002>.
- [10] L.P. Christopher, Hemanathan Kumar, V.P. Zambare, Enzymatic biodiesel: challenges and opportunities, *Appl. Energy* 119 (2014) 497–520, <https://doi.org/10.1016/j.apenergy.2014.01.017>.
- [11] B. Likozar, A. Pohar, J. Levec, Transesterification of oil to biodiesel in a continuous tubular reactor with static mixers: modelling reaction kinetics, mass transfer, scale-up and optimization considering fatty acid composition, *Fuel Process. Technol.* 142 (2016) 326–336, <https://doi.org/10.1016/j.fuproc.2015.10.035>.
- [12] I. Lee, L.M. Pfalzgraf, G.B. Poppe, E. Powers, T. Haines, The role of sterol glucosides on filter plugging, *Biodiesel Mag* 4 (2007) 105–112.
- [13] V. Van Hoed, N. Zaykina, W. De Greyt, J. Maes, R. Verhé, K. Demeestere, Identification and occurrence of sterol glucosides in palm and soy biodiesel, *JAACS, J. Am. Oil Chem. Soc.* 85 (2008) 701–709, <https://doi.org/10.1007/s11746-008-1263-5>.
- [14] R.A. Moreau, K.M. Scott, M.J. Haas, The identification and quantification of sterol glucosides in precipitates from commercial biodiesel, *JAACS, J. Am. Oil Chem. Soc.* 85 (2008) 761–770, <https://doi.org/10.1007/s11746-008-1264-4>.
- [15] H. Tang, S.O. Salley, K.Y. Simon Ng, Fuel properties and precipitate formation at low temperature in soy-, cottonseed-, and poultry fat-based biodiesel blends, *Fuel* 87 (2008) 3006–3017, <https://doi.org/10.1016/j.fuel.2008.04.030>.
- [16] D. Na-Ranong, P. Laungthaleongpong, S. Khambung, Removal of sterol glucosides in palm oil based biodiesel using magnesium silicate and bleaching earth, *Fuel* 143 (2015) 229–235, <https://doi.org/10.1016/j.fuel.2014.11.049>.
- [17] A. Aguirre, S. Peiru, F. Eberhardt, L. Vetcher, R. Cabrera, H.G. Menzella, Enzymatic hydrolysis of sterol glucosides, major contaminants of vegetable oil-derived biodiesel, *Appl. Microbiol. Biotechnol.* 98 (2014) 4033–4040, <https://doi.org/10.1007/s00253-013-5345-4>.
- [18] S. Peiru, A. Aguirre, F. Eberhardt, M. Braia, R. Cabrera, H.G. Menzella, An industrial scale process for the enzymatic removal of sterol glucosides from biodiesel, *Biotechnol. Biofuels* 8 (2015), <https://doi.org/10.1186/s13068-015-0405-x>.
- [19] A.Y. Tremblay, A. Montpetit, The in-process removal of sterol glucosides by ultrafiltration in biodiesel production, *Biofuel Res. J.* 4 (2017) 559–564, <https://doi.org/10.18331/brj2017.4.1.6>.
- [20] M.Y. Chang, R.S. Juang, Adsorption of tannic acid, humic acid, and dyes from water using the composite of chitosan and activated clay, *J. Colloid Interface Sci.* 278 (2004) 18–25, <https://doi.org/10.1016/j.jcis.2004.05.029>.
- [21] A.G. Varghese, S.A. Paul, M.S. Latha, Green Adsorbents for Pollutant Removal, 2018, <https://doi.org/10.1007/978-3-319-92111-2>.
- [22] M. Börjesson, G. Westman, Crystalline nanocellulose — preparation, modification, and properties, *Cellul. - Fundam. Asp. Curr. Trends.* (2015), <https://doi.org/10.5772/61899>.
- [23] H. Voisin, L. Bergström, P. Liu, A. Mathew, Nanocellulose-based materials for water purification, *Nanomaterials* 7 (2017) 57, <https://doi.org/10.3390/nano7030057>.
- [24] H. Liang, X. Hu, A quick review of the applications of nano crystalline cellulose in wastewater treatment, *J. Bioresour. Bioprod.* (2016) 199–204, 2016, www.Bioresources-Bioproducs.com.
- [25] J.N. Putro, S.P. Santoso, S. Ismadji, Y.H. Ju, Investigation of heavy metal adsorption in binary system by nanocrystalline cellulose – bentonite nanocomposite: improvement on extended Langmuir isotherm model, *Microporous Mesoporous Mater.* 246 (2017) 166–177, <https://doi.org/10.1016/j.micromeso.2017.03.032>.
- [26] L. Segal, J.J. Creely, A.E. Martin, C.M. Conrad, An empirical method for estimating the degree of crystallinity of native cellulose using the X-ray diffractometer, *Textil. Res. J.* 29 (1959) 786–794, <https://doi.org/10.1177/004051755902901003>.
- [27] L. Nyström, Occurrence and Properties of Steryl Ferulates and Glycosides in Wheat and Rye, University of Helsinki, 2007.
- [28] L.B.D.C. Araújo, S.L. Silva, M.A.M. Galvão, M.R.A. Ferreira, E.L. Araújo, K.P. Randau, L.A.L. Soares, Total phytosterol content in drug materials and extracts from roots of *Acanthospermum hispidum* by UV-VIS spectrophotometry, *Brazilian J. Pharmacogn.* 23 (2013) 736–742, <https://doi.org/10.1590/S0102-695X2013000500004>.
- [29] M.N.A.M. Taib, W.A. Yehye, N.M. Julkapli, Influence of crosslinking density on antioxidant nanocellulose in bio-degradation and mechanical properties of nitrile rubber composites, *Fibers Polym.* 20 (2019) 165–176, <https://doi.org/10.1007/s12221-019-8575-y>.
- [30] Y. Hu, L. Tang, Q. Lu, S. Wang, X. Chen, B. Huang, Preparation of cellulose nanocrystals and carboxylated cellulose nanocrystals from borer powder of bamboo, *Cellulose* 21 (2014) 1611–1618, <https://doi.org/10.1007/s10570-014-0236-0>.
- [31] A. Alemdar, M. Sain, Isolation and characterization of nanofibers from agricultural residues - wheat straw and soy hulls, *Bioresour. Technol.* 99 (2008) 1664–1671, <https://doi.org/10.1016/j.biortech.2007.04.029>.
- [32] X.F. Sun, F. Xu, R.C. Sun, P. Fowler, M.S. Baird, Characteristics of degraded cellulose obtained from steam-exploded wheat straw, *Carbohydr. Res.* 340 (2005) 97–106, <https://doi.org/10.1016/j.carres.2004.10.022>.
- [33] H. Wang, H. Tang, S. Salley, K.Y. Simon Ng, Analysis of sterol glucosides in biodiesel and biodiesel precipitates, *JAACS, J. Am. Oil Chem. Soc.* 87 (2010) 215–221, <https://doi.org/10.1007/s11746-009-1489-x>.
- [34] N.A. Negm, M.T.H. Abou Kana, M.A. Youssif, M.Y. Mohamed, Biofuels from Vegetable Oils as Alternative Fuels: Advantages and disadvantages, 2017, <https://doi.org/10.1201/b20780>.
- [35] A. Khodabandehloo, A. Rahbar-Kelishami, H. Shayesteh, Methylene blue removal using *Salix babylonica* (Weeping willow) leaves powder as a low-cost biosorbent in batch mode: kinetic, equilibrium, and thermodynamic studies, *J. Mol. Liq.* 244 (2017) 540–548, <https://doi.org/10.1016/j.molliq.2017.08.108>.
- [36] H.J. Lee, H.S. Lee, J. Seo, Y.H. Kang, W. Kim, T.H.K. Kang, State-of-the-art of cellulose nanocrystals and optimal method for their dispersion for construction-related applications, *Appl. Sci.* 9 (2019) 1–14, <https://doi.org/10.3390/app9030426>.
- [37] S. Chowdhury, R. Mishra, P. Saha, P. Kushwaha, Adsorption thermodynamics, kinetics and isosteric heat of adsorption of malachite green onto chemically modified rice husk, *Desalination* 265 (2011) 159–168, <https://doi.org/10.1016/j.desal.2010.07.047>.
- [38] H. More, Factors Affecting Adsorption. <https://hemantmore.org.in/science/chemistry/factors-affecting-adsorption/13094/>, 2018 accessed May 5, 2019.
- [39] M. Mohapatra, S. Khatun, S. Anand, Kinetics and thermodynamics of lead (II) adsorption on lateritic nickel ores of Indian origin, *Chem. Eng. J.* 155 (2009) 184–190, <https://doi.org/10.1016/j.cej.2009.07.035>.
- [40] A. de Sá, A.S. Abreu, I. Moura, A.V. Machado, Polymeric Materials for Metal Sorption from Hydric Resources, Elsevier Inc., 2017, <https://doi.org/10.1016/b978-0-12-804300-4.00008-3>.
- [41] C.S. Zhu, L.P. Wang, W. bin Chen, Removal of Cu(II) from aqueous solution by agricultural by-product: peanut hull, *J. Hazard Mater.* 168 (2009) 739–746, <https://doi.org/10.1016/j.jhazmat.2009.02.085>.
- [42] Q. Li, L. Chai, Z. Yang, Q. Wang, Kinetics and thermodynamics of Pb(II) adsorption onto modified spent grain from aqueous solutions, *Appl. Surf. Sci.* 255 (2009) 4298–4303, <https://doi.org/10.1016/j.apsusc.2008.11.024>.
- [43] Y. Liu, Y.J. Liu, Biosorption isotherms, kinetics and thermodynamics, *Separ. Purif. Technol.* 61 (2008) 229–242, <https://doi.org/10.1016/j.seppur.2007.10.002>.
- [44] Y. Habibi, L.A. Lucia, O.J. Rojas, Cellulose nanocrystals: chemistry, self-assembly, and applications, *Chem. Rev.* 110 (2010) 3479–3500, <https://doi.org/10.1021/cr900339w>.
- [45] Y. Liu, D. Ying, L. Sanguansri, Y. Cai, X. Le, Adsorption of catechin onto cellulose and its mechanism study: kinetic models, characterization and molecular simulation, *Food Res. Int.* 112 (2018) 225–232, <https://doi.org/10.1016/j.foodres.2018.06.044>.